PHYSICAL REVIEW MATERIALS **00**, 003600 (2021)

Defect chemistry of Cr-B binary and Cr-Al-B MAB phases: Effects of covalently bonded B networks

Jun Young Kim [1,2,*] Jianqi Xi,[1] Hongliang Zhang [3] and Izabela Szlufarska[1,†]

[1]*Department of Materials Science and Engineering, University of Wisconsin–Madison, Madison, Wisconsin 53706, USA*

[2]*Department of Electrical and Computer Engineering, University of Wisconsin–Madison, Madison, Wisconsin 53706, USA*

[3]*Department of Engineering Physics, University of Wisconsin–Madison, Madison, Wisconsin 53706, USA*

(Received 14 May 2021; revised 19 September 2021; accepted 12 October 2021; published xxxxxxxxxx)

Transition metal borides, which are three-dimensional (3D) layered materials containing covalently bonded B networks, have shown a number of excellent properties, such as radiation resistance and the ability to act as a diffusion barrier in integrated circuits. However, defect behavior, which controls many of the materials' properties, has remained unknown in these materials. Here, we investigate the effects of the B networks on the defect chemistry in both binary borides (CrB, Cr_3B_4, Cr_2B_3) and ternary MAB phases (Cr_2AlB_2, Cr_3AlB_4, Cr_4AlB_6) using first-principles calculations. We find that increasing the number of B rings in the structure leads to lower formation energies and higher concentrations of Frenkel pairs. The results can be explained by the fact that the strongest Cr-B bond is weakened when borides have more B rings, leading to a reduction in the formation energy of Cr and B vacancies. Also, the bonds associated with Cr atoms bonded within B rings are softer in structures containing more B rings, which allows Cr interstitials to form with a lower energy cost and contributes to an increase in the concentration of Cr interstitials.

DOI: 10.1103/PhysRevMaterials.00.003600

I. INTRODUCTION

Binary transition metal borides have been shown to exhibit many outstanding properties due to the presence of covalently bonded B networks bonded to transition metals. These properties include high melting point, high decomposition temperature, and high hardness and strength [1,2]. However, applications of binary transition metal borides have been limited because of their poor tolerance to oxidation and thermal shock as well as intrinsic brittleness and poor machinability [3]. Recently, layered ternary transition metal borides called MAB phases (M: transition metal; A: group III-A elements; B: B) have been found to exhibit excellent properties, such as hardness [4,5], thermal and electrical conductivities [6,7], magnetocaloric effect [8], oxidation resistance [9,10], and radiation tolerance [11]. Moreover, MBenes, exfoliated from bulk MAB phases, have emerged as promising two-dimensional materials in applications such as spintronic devices [12].

To make use of and to control the outstanding properties of the transition metal borides, one has to take into account defects because a finite concentration of defects always exists and often governs material properties. For instance, deintercalation of Al, a proposed pathway to the exfoliation of MBenes from MAB phases, involves the formation of stacking faults [13]. In the field of nuclear materials, it has been recently reported that unstable Mo interstitials in MoAlB create Mo_{Al} antisites that cannot be recovered easily and lead to the poor tolerance of this particular MAB phase to radiation-induced amorphization [11]. In integrated circuits, where Cr-B binaries can be used as diffusion barriers [14], understanding defect behavior is also critical since impurity diffusion is often vacancy mediated [15].

The goal of the current study is to bring insights into how defect stability and concentrations depend on the atomic structure of the transition metal borides. In particular, we have chosen three binary Cr-B systems (CrB, Cr_3B_4, Cr_2B_3) and three Cr-Al-B MAB phases (Cr_2AlB_2, Cr_3AlB_4, Cr_4AlB_6). These materials have been chosen for a few different reasons. First of all, Cr-B systems have been used for high-temperature applications, including diffusion barriers for integrated circuits [14] and wear-resistant coatings [16]. Secondly, varying the composition while keeping the elements the same allows us to study how defect stability depends on different B networks, with the goal of extracting more general rules. Specifically, as depicted in Fig. 1, B atoms in CrB and Cr_2AlB_2 form a single B chain and Cr_3B_4 and Cr_3AlB_4 contain two B chains that form a single layer of B rings, whereas Cr_2B_3 and Cr_4AlB_6 have three B chains that form two-B-ring layers. Cr_2AlB_2, Cr_3AlB_4, and Cr_4AlB_6 are similar to CrB, Cr_3B_4, and Cr_2B_3, respectively, except for the addition of the Al layers interleaving the Cr-B units. This set of the six borides provides a testbed for understanding the effects of covalent B rings (i.e., B chain vs one B ring vs two B ring) on the formation of defects. In this report, we use density functional theory (DFT) to investigate the defect chemistry of the six borides and the effects of atomic structure on the formation energies and concentrations of defects.

II. METHODS

DFT calculations were performed using the Vienna *ab initio* simulation package [17] with the projector augmented wave [18] and the generalized gradient approximation by

*kim792@wisc.edu
†szlufarska@wisc.edu

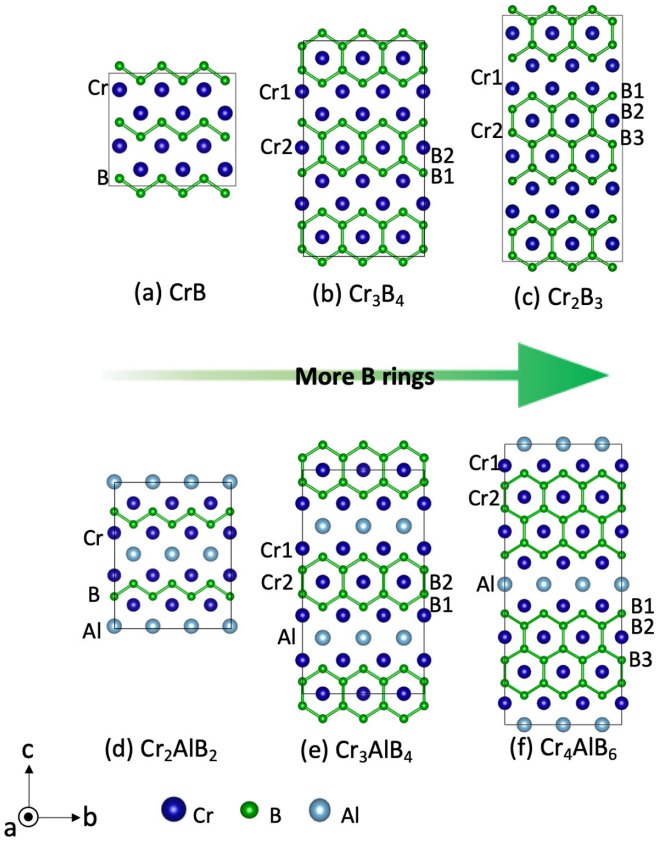

FIG. 1. Supercell for (a) CrB, (b) Cr_3B_4, (c) Cr_2B_3, (d) Cr_2AlB_2, (e) Cr_3AlB_4, and (f) Cr_4AlB_6.

Perdew, Burke, and Ernzerhof [19]. The plane-wave cutoff energy of 400 eV and the energy tolerance of 0.5 meV/atoms were used. For the six systems, different Monkhorst-Pack k-point mesh sizes were used to optimize the geometry [20]: CrB, Cr_3B_4, Cr_2AlB_2 ($7 \times 7 \times 5$) and Cr_2B_3, Cr_3AlB_4, Cr_4AlB_6 ($9 \times 9 \times 3$). The total energies of perfect structures as well as the energies of structures containing either a vacancy or an antisite were calculated in $3 \times 3 \times 2$ supercells for CrB, Cr_3B_4, Cr_2AlB_2, and Cr_3AlB_4 and $3 \times 3 \times 1$ supercells for Cr_2B_3 and Cr_4AlB_6. Interstitial calculations required bigger supercells, which were determined based on the results of convergence tests. To take into account the magnetic properties of Cr-(Al)-B systems [21], the magnetic moment was included in the DFT calculations.

The enthalpy of formation H_f for a defect is calculated as

$$H_f = [E_d + \Delta H_d(T, p^0)] - [E_p + \Delta H_p(T, p^0)] - \sum_i n_i \mu_i(T), \quad (1)$$

where the subscripts d and p denote defective and perfect crystals, respectively, and E is the total energy at 0 K. ΔH is the change in enthalpy at the standard pressure, which is approximately identical in a defective system and a perfect system and thus is assumed to be canceled out. In addition, the change in volume due to formation of a defect is assumed to be negligible. In Eq. (1), n_i is the number of atoms removed or added when introducing a defect, and the chemical potential μ_i is calculated using the following equation:

$$\mu_i(T) = \mu_i^{\text{ref}} + \Delta\mu_i + \Delta H_i(T, p^0). \quad (2)$$

Here, μ^{ref} is the reference chemical potential obtained from a bulk system at 0 K, ΔH is the change in enthalpy at the standard pressure obtained from the JANAF thermochemical tables [22], and $\Delta\mu$ is the change in the chemical potential with respect to its reference state. We provided $\Delta\mu$ values for Cr- and B-rich conditions in Tables SI and SII in the Supplemental Material [23]. We also fixed the change in the chemical potential of Al at Al-rich condition ($\Delta\mu_{\text{Al}} = 0$), based on the information that MAB phases are synthesized in Al-rich conditions [4]. The enthalpy of formation H_f is used to calculate the defect concentration (c) using the following equation,

$$c = N_d \exp\left(-\frac{G_f}{k_B T}\right) = N_d \exp\left(-\frac{H_f - TS_f}{k_B T}\right), \quad (3)$$

where N_d is the number of available sites for the formation of a given defect per unit volume, k_B is the Boltzmann constant, and S_f is the entropy of formation. The entropy calculation is costly, especially for the large systems (e.g., Cr_2B_3 and Cr_4AlB_6) and for calculations of interstitials, which require large supercell sizes based on our convergence tests. Previous studies have shown that experimental and theoretical results for the entropy of formation of a point defect typically range from 0 to 10 k_B, and therefore the entropy term S_f has been often neglected when calculating concentrations of point defects [23–27]. In addition, here, we compared the Gibbs free energy of formation and the enthalpy of formation for selected defects and we found the difference between the Gibbs free energy and the enthalpy to be smaller than 0.03 eV (see Fig. S1 in the Supplemental Material [23]). In the Supplemental Material, we have further shown that the entropy contribution is negligible relative to the enthalpy difference even at elevated temperatures. For the entropy calculations, we used PHONOPY, an open source package for phonon calculations [29–31].

To investigate the role of the strength of chemical bonds, in this study we calculate the bond separation energy at 0 K. This is done by subtracting the energy of a perfect unit cell from the energy of a unit cell where a vacuum region of 2 nm thickness is inserted between the layers and finally by dividing the energy difference by the number of surface atoms. We did not relax atoms to calculate the bond separation energy. Using a finite-displacement scheme, we also calculated dynamical matrices, from which we extracted interatomic force constants.

III. RESULTS AND DISCUSSION

The calculated lattice constants (a, b, c) of each system are: CrB (2.90, 2.89, 7.72 Å), Cr_3B_4 (2.88, 2.92, 12.88 Å), Cr_2B_3 (2.90, 2.93, 17.98 Å), Cr_2AlB_2 (2.91, 2.90, 10.86 Å), Cr_3AlB_4 (2.91, 2.92, 7.98 Å), and Cr_4AlB_6 (2.91, 2.93, 21.01 Å). All of these are in good agreement with reported experiments [4,32]. The formation enthalpy of each system was calculated to be CrB (−1.72 eV/f.u.), Cr_3B_4 (−5.67 eV/f.u.), Cr_2B_3 (−3.95 eV/f.u.), Cr_2AlB_2 (−3.95 eV/f.u.), Cr_3AlB_4 (−6.16 eV/f.u.), and Cr_4AlB_6 (−8.69 eV/f.u.). These values

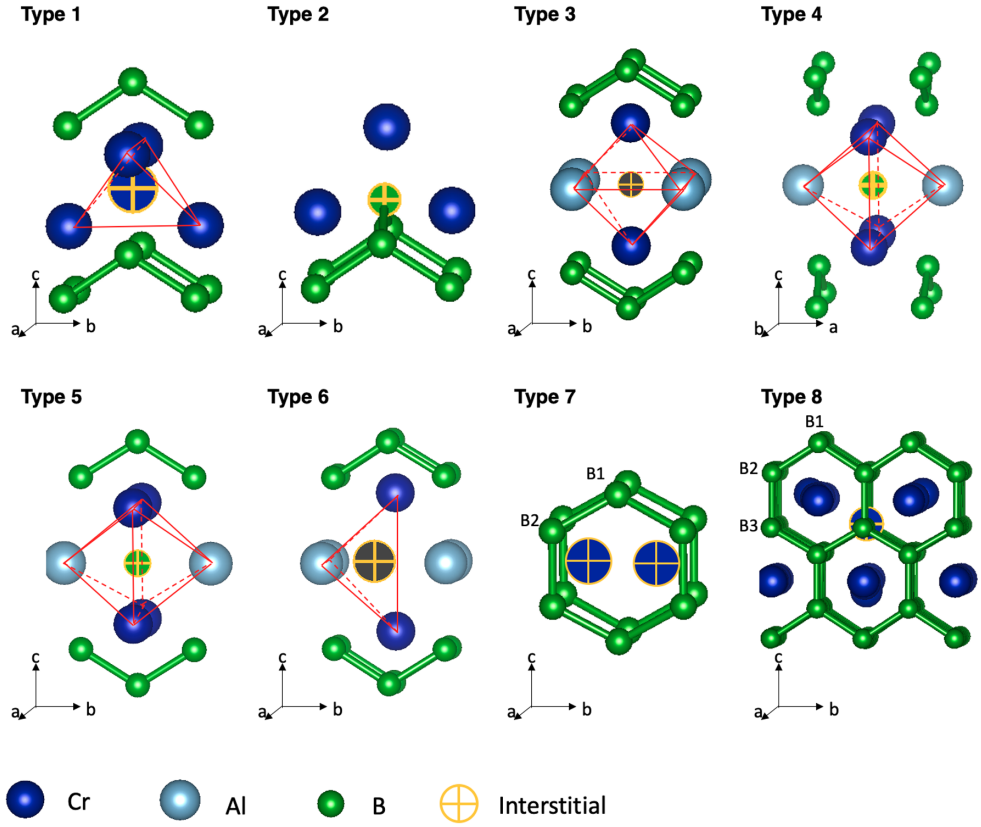

FIG. 2. Types of the most stable interstitials in binary and ternary borides.

were used to determine the change in chemical potential with respect to its reference state at Cr- and B-rich conditions (see Supplemental Material [23] for the details of the calculations and the calculated values).

While vacancy and antisite defects are located at lattice sites, several different off-lattice sites are found for stable interstitials. Figure 2 shows the types of the most stable interstitials. The interstitial types that are less stable are depicted in Fig. S4 in the Supplemental Material [23], and the defect formation energies are provided in Table SIII [23]. In CrB, the only stable site for the Cr interstitial was found at the center of a tetrahedron composed of four Cr atoms outside B-chain layers (type 1 in Fig. 2). B interstitials in CrB form two types of B bridges: The more stable type (type 2 in Fig. 2) involves the interstitial connecting two different B chains and the other interstitial type (type 9 in Fig. S4 [23]) bonds with two B atoms within a B chain. In Cr_3B_4 and Cr_2B_3, as shown in Fig. 1, there are different inequivalent lattice sites within a unit cell where Cr and B vacancies can form (Cr1, Cr2, B1, B2, and/or B3). Both Cr and B vacancies are found to have lower formation energies when forming within B-ring layers. The most stable Cr and B vacancies, respectively, are V_{Cr2} and V_{B2} in Cr_3B_4 and V_{Cr2} and V_{B3} in Cr_2B_3. For Cr interstitials in Cr_3B_4 and Cr_2B_3, the most stable interstitials were found within B-ring layers. As shown in Fig. 2, the most stable Cr interstitial in Cr_3B_4 forms a Cr dumbbell aligned along the *b* axis within a B-ring layer (type 7), and the most stable Cr interstitial in Cr_2B_3 forms in between two B3 atoms (type 8 in Fig. 2). In Cr_3B_4 and Cr_2B_3, the type 2 B interstitial was found as the most stable B interstitial in each system, while type 9 (shown in Fig. S4 [23]) was found only in Cr_3B_4. B interstitials are also found to form within B-ring layers of Cr_3B_4 and Cr_2B_3, but their formation energies are higher than the most stable B interstitial in the respective system at least by 0.7 eV (see Table SIII [23]).

In Cr_2AlB_2, the only stable configuration of the Cr interstitial was found at the center of an octahedron composed of two Cr atoms and four Al atoms (type 3 in Fig. 2), and the most stable Al interstitial was found at the center of an octahedron composed of two Al atoms and four Cr atoms (type 4 in Fig. 2). In Cr_2AlB_2, three types of B interstitials were found within Al layers at the center of octahedrons as shown in Fig. 2: at the center of an octahedron composed of four Al atoms and two Cr atoms (type 3), at the center of an octahedron composed of two Al atoms (aligned along the *a* axis) and four Cr atoms (type 4), and at the center of an octahedron composed of two Al atoms (aligned along the *b* axis) and four Cr atoms (type 5). Among the three types of B interstitials, type 4 is the most stable. In Cr_3AlB_4 and Cr_4AlB_6, similarly to Cr and B vacancies in the corresponding binaries, the most stable vacancies are V_{Cr2} and V_{B2} in Cr_3AlB_4 and V_{Cr2} and V_{B3} in Cr_4AlB_6, all of which form within B-ring layers. In Cr_3AlB_4 and Cr_4AlB_6, the most stable Cr interstitials form within Al layers as a tetrahedron composed of two Cr atoms and two Al atoms (type 6 in Fig. 2). Although Cr interstitials are also found within B-ring layers in Cr_3AlB_4 and Cr_4AlB_6, their formation energies are much higher than that of the type 6 Cr interstitial (see Table SIII [23]). Al interstitials are similar—the most stable Al interstitials were found within Al layers (type 6 in Fig. 2) and are significantly more stable than

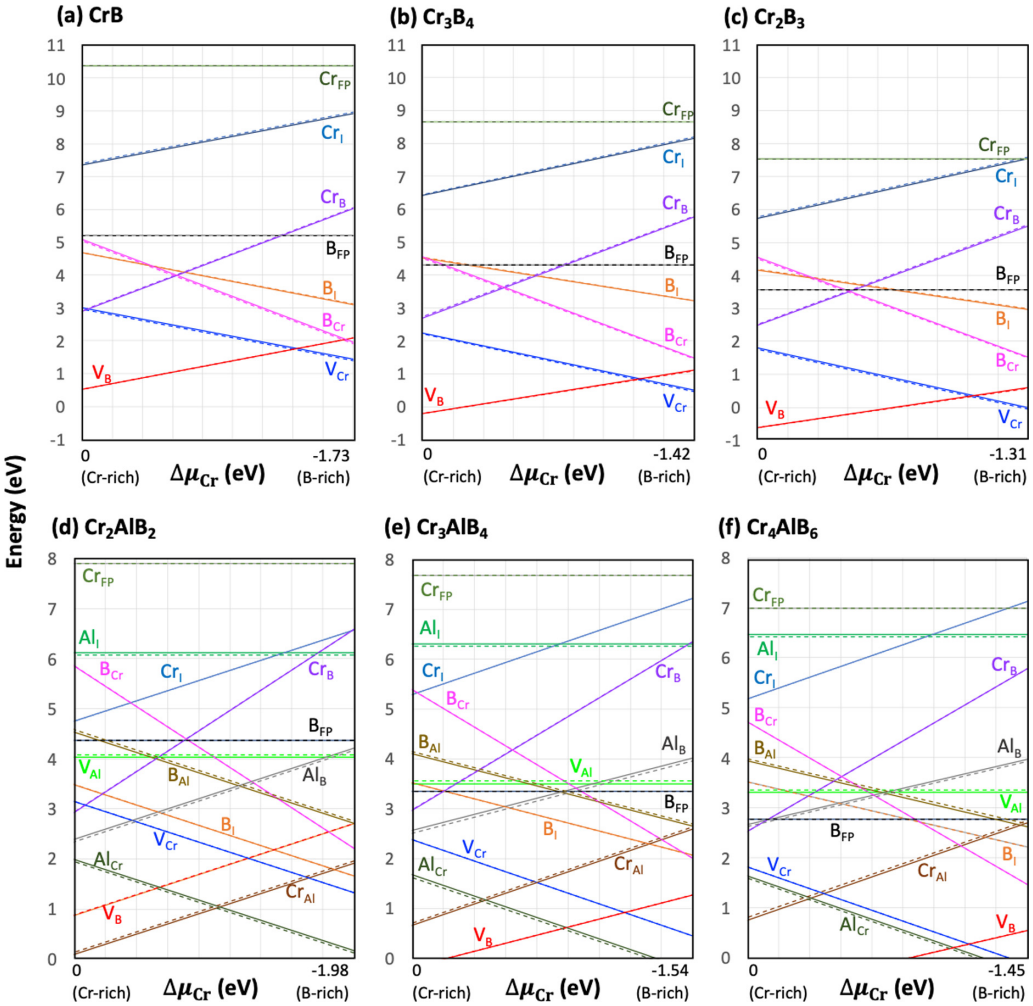

FIG. 3. Defect formation energies at 0 K (bold) and 300 K (dashed) in (a) CrB, (b) Cr_3B_4, (c) Cr_2B_3, (d) Cr_2AlB_2, (e) Cr_3AlB_4, and (f) Cr_4AlB_6.

the other Al interstitials found within B-ring layers (see Table SIII [23]). As for B interstitials in Cr_3AlB_4 and Cr_4AlB_6, they are similar to the B interstitials in Cr_2AlB_2. The stable B interstitials are found in Al layers at the center of an octahedron as shown in Fig. 2: type 3, type 4, and type 5. The formation energies of the B interstitials found within B-ring layers are much higher than those of the three types of B interstitials found in Al layers (see Table SIII [23]).

To summarize, in CrB where B atoms form B chains, Cr and B vacancies are allowed to form at only one site for each species, whereas in the systems where B atoms form B rings (Cr_3B_4 and Cr_2B_3) the most stable Cr and B vacancies form within B-ring layers. As for interstitials in the binaries, the only Cr interstitial in CrB is found outside B-chain layers (type 1 in Fig. 2), while the most stable Cr interstitials are found within B-ring layers in Cr_3B_4 and Cr_2B_3. In the binaries, the most stable B interstitials are all found to form a B bridge (type 2 in Fig. 2). For the ternaries, in Cr_2AlB_2 (which has B-chain layers), Cr and B vacancies form at only one site for each of the species, whereas in the systems that have B-ring layers (Cr_3AlB_4 and Cr_4AlB_6) the most stable Cr and B vacancies form within the B-ring layers. All the most stable interstitials in the ternaries are found within Al layers. As such, the types of defects created are different in the six borides and they are associated with the B-ring layers. Therefore, for applications of the borides, it is critical to understand the dependence of the defect formation on the number of B-ring layers in the binary Cr-B systems and the ternary Cr-Al-B MAB phases. Here, we will investigate the question of how the defect formation energies and the defect concentrations change with an increasing number of B-ring layers.

The formation energies of the most stable point defects and Frenkel pairs (FPs) at 0 and 300 K are plotted as a function of the chemical potential in Fig. 3. We also provided the concentrations of the defects in Fig. S5 in the Supplemental Material [23] and N_d used to calculate the concentrations in Table SIV [23]. For the ternary systems, the defect formation energies were calculated at the Al-rich conditions because Cr-Al-B MAB phases are synthesized in Al-rich environments [4]. For each type of defect, the defect with the lowest formation energy is found to be the defect with the highest concentration.

To investigate the effects of the number of B rings on the defect formation energies (i.e., B chain vs one-B ring vs two-B ring), we compare the formation energies of vacancies,

TABLE I. Bond separation energy in the six borides shown in Fig. 1.

	Bond separation energy (eV)					
	CrB	Cr_3B_4	Cr_2B_3	Cr_2AlB_2	Cr_3AlB_4	Cr_4AlB_6
Cr1-Cr1[a]	4.38	4.21	4.14	N/A	N/A	N/A
Cr1-B1[a]	6.33	6.03	6.19	6.24	5.86	6.10
B1-B2[a]	4.82	4.99	4.96	5.05	5.19	5.14
Cr1-Al	N/A	N/A	N/A	3.33	3.37	3.42
Cr2-B2	N/A	5.44	5.30	N/A	5.57	5.41
Cr2-B3	N/A	N/A	5.11	N/A	N/A	5.01
B3-B3	N/A	N/A	5.25	N/A	N/A	5.29

[a]Cr1 for CrB and Cr_2AlB_2 denotes Cr, and B1 and B2 for CrB and Cr_2AlB_2 denote B, as depicted in Figs. 1(a) and 1(d).

interstitials, and FPs in the binaries first (CrB, Cr_3B_4, Cr_2B_3). Figures 3(a)–3(c) show that the defect formation energies of V_B (red) and V_{Cr} (blue) decrease from CrB to Cr_3B_4 and to Cr_2B_3, which is the order of increasing the number of B rings. The defect formation energies plotted for B vacancy correspond to V_{B2} in Cr_3B_4 and V_{B3} in Cr_2B_3, and the defect formation energies plotted for Cr vacancy correspond to V_{Cr2} for both Cr_3B_4 and Cr_2B_3. The decrease in defect formation energies of V_B and V_{Cr} is attributed to the weakening of the strongest Cr-B bond from CrB to Cr_3B_4 and to Cr_2B_3. Kádas *et al.* have previously shown that the M-B bond is the strongest bond in M_2AlB_2 (M = Cr, Mn, Fe, and Co) systems. The authors have also found that the work of separation can be used as a reliable measure of the bond strength in MAB phases [33]. For that reason and because of the computational efficiency of such approach, here we also use the work of separation to determine qualitative trends in the bond strengths in Cr-B and Cr-Al-B systems. The work of separation is calculated using DFT and the results are shown in Table I. The work of separation for the Cr-B bond in CrB is 6.33 eV (Cr1-B1 in Table I), in Cr_3B_4 it is 5.44 eV (Cr2-B2), and in Cr_2B_3 it is 5.30 eV (Cr2-B2) and 5.11 eV (Cr2-B3). These data show that, when B networks contain more B rings (from B chain to one-B ring, and to two-B ring), the Cr-B bond (the strongest bond in the systems) is weakened and consequently Cr and B vacancies are easier to form.

As shown in Figs. 3(a)–3(c), the defect formation energies of Cr_I (sky blue) in the binaries decrease with an increase in the number of B rings. In CrB, the only stable site for the Cr interstitial is at the center of a tetrahedron composed of four Cr atoms (type 1 in Fig. 2) outside B-chain layers. In Cr_3B_4, the most stable Cr interstitial forms a Cr dumbbell on a Cr2 site (type 7 in Fig. 2), and in Cr_2B_3, the most stable Cr interstitial forms in between two B3 atoms (type 8 in Fig. 2). Note that Cr interstitials in Cr_3B_4 and Cr_2B_3 are found within B-ring layers. The decrease in the defect formation energy of Cr_I in Figs. 3(a)–3(c) is due to the softness of the bonds associated with Cr2 atoms positioned within B-ring layers, which helps accommodate interstitials more easily. To show this, we plotted the force constants of Cr1 and Cr2 in each system. The force constant in the in-plane direction is defined as the average of the force constants along the *b* and *c* axes, and the out-of-plane direction constant is defined as a constant along the *c* axis (the axes are indicated in Fig. 1). The force constants for Cr2 are much lower than those for Cr1 in the binary borides. This trend indicates that Cr2 atoms relax more easily than Cr1 atoms do, which allows the systems having Cr2 atoms (and hence, having B-ring layers) to accommodate interstitials with a lower energy cost. As for the B interstitials in the binaries, the defect formation energies of B_I (orange) change only a little over the different systems, because B_I's share the same type of B-bridge structure (type 2 in Fig. 2), and the distances between the B interstitial and the nearest B atom differ only with the standard deviation of 0.01 Å.

As mentioned in the Introduction, Cr_2AlB_2 (B chain), Cr_3AlB_4 (one-B ring), and Cr_4AlB_6 (two-B ring) are similar in structure to CrB, Cr_3B_4, and Cr_2B_3, respectively, except for the addition of the Al layers. Here, we compare the formation energies of defects in the ternaries and investigate the effects of the number of B rings. The formation energies of defects in Cr_2AlB_2, Cr_3AlB_4, and Cr_4AlB_6 are plotted in Figs. 3(d)–3(f). For Cr and B vacancies, we found the same trend as in the binary systems. The formation energies of V_{Cr} (blue) and V_B (red) in Figs. 3(d)–3(f) decrease with an increasing number of B rings (from Cr_2AlB_2 to Cr_3AlB_4 and to Cr_4AlB_6) and this trend can be attributed to weakening of the Cr-B bond. This weakening is evidenced by the calculated bond separation energy: The Cr-B bond separation energy relevant to the formation of V_{Cr} and V_B in Cr_2AlB_2 is 6.24 eV (Cr1-B1), whereas in Cr_3AlB_4 it is 5.57 eV (Cr2-B2) and in Cr_4AlB_6 it is 5.41 eV (Cr2-B2) and 5.01 eV (Cr2-B3). The defect formation energy of V_{Al} (lime) was also found to decrease with an increase in the number of B rings.

The most stable Cr, Al, and B interstitials in the ternaries were all found within Al layers. This is because of the softness of the Al layers, whose in-plane force constants (determined as the average of the *a*-axis and *b*-axis constants) range from 115 to 118 N/m over the three ternaries. These force constants are even lower than those of Cr2 atoms in B-ring layers (see Fig. 4), which is why the most stable interstitials form within Al layers in the ternaries rather than in the B-ring layers. The defect formation energies of Cr_I, Al_I, and B_I in Cr_3AlB_4 and Cr_4AlB_6 are slightly higher than those in Cr_2AlB_2. This higher formation energy can be explained by the differences in the thickness of the Cr-Al-Cr layer where the interstitials are accommodated. Zhao *et al.* pointed out that a bigger interlayer spacing in MAX phase Ti_3AlC_2 provides an interstitial with more stable sites, leading to a lower formation energy as compared with MAX phase Ti_3SiC_2 [34]. In the case of MAB phases studied here, our DFT calculations show that in the relaxed undefected structures, the interlayer spacing of Cr-Al-Cr (where the interstitials would reside) is 3.27 Å (Cr_2AlB_2), 3.21 Å (Cr_3AlB_4), and 3.22 Å (Cr_4AlB_6). The interlayer spacings of Cr_3AlB_4 and Cr_4AlB_6 are slightly smaller than that of Cr_2AlB_2, which is consistent with the higher formation energies of the interstitials in Cr_3AlB_4 and Cr_4AlB_6.

To summarize, in the binaries, increasing the number of B rings in the structure leads to lower formation energies (and hence higher concentrations) of V_B, V_{Cr}, and Cr_I, whereas the formation energies of B_I are not significantly affected. This trend suggests the easier formation of FPs and the increase in the concentrations of B FPs and Cr FPs in the binaries [Figs. 3(a)–3(c)]. In the ternaries, increasing the number of

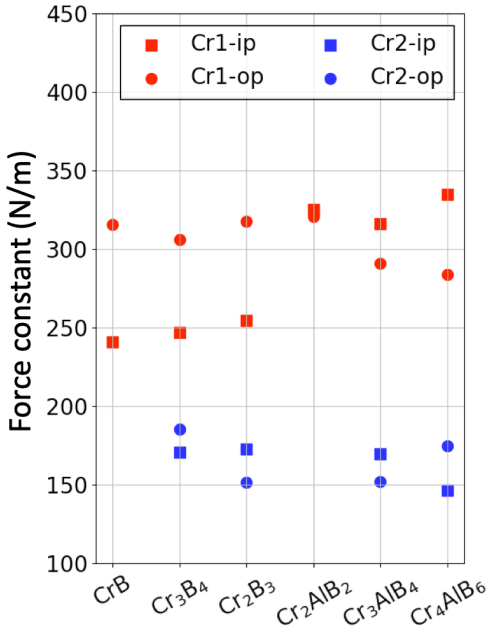

FIG. 4. Force constants of Cr1 and Cr2 in the in-plane direction (ip) and out-of-plane direction (op).

B rings is associated with significant decreases in formation energies (and hence increases in concentrations) of vacancies and slight increases in interstitial formation energies [see Figs. 3(d)–3(f)]. Therefore, the easier formation of FPs and the corresponding increase in concentrations of Cr and B FPs are expected with increasing the number of B rings. These trends indeed are found in our data, as shown in Figs. 3(d)–3(f) and Figs. S5(d)–S5(f) [23].

It is interesting to consider how the effects of B rings on defect formation energy and concentration could relate to applications of the borides. In integrated circuit applications, for diffusion barriers to prevent Cu atoms from diffusing out, barrier metals should have a high diffusion energy barrier or a high vacancy formation energy (low concentration) [15]. Based on our results, the vacancy formation energies are lower (the defect concentrations are higher) when a system has more B rings. This result implies that Cr_3B_4, Cr_2B_3, Cr_3AlB_4, and Cr_4AlB_6 contain more vacancies via which Cu atoms can diffuse and that, at least based on the defect concentrations, CrB and Cr_2AlB_2 might be more effective as diffusion barrier materials. For nuclear reactor applications, understanding defect behavior is critical. Under radiation, a large number of FPs are created, and a material's tolerance to radiation-induced amorphization largely depends on how many defects are created and how many of them are removed through defect recovery processes [11]. The radiation-induced defect recovery process involves complex processes, the understanding of which requires formation energies as the first step. For example, in this work, we found that the most stable B interstitial and vacancy in Cr_2B_3 and Cr_4AlB_6 are separated spatially from each other. That could potentially lead to a non-negligible energy barrier to recombination and could contribute to the accumulation of radiation-induced damage. The kinetics of defects needs to be further investigated to ultimately determine their impact on the recovery process. Our data on concentrations combined with future studies of kinetics will be important for boride applications including diffusion barrier and nuclear reactor applications.

IV. CONCLUSION

We investigated defect chemistry in CrB, Cr_3B_4, Cr_2B_3, Cr_2AlB_2, Cr_3AlB_4, and Cr_4AlB_6 by calculating the defect formation energies and concentrations of point defects and FPs using DFT. We discussed the effects of the number of B rings on the defect formation energies and the defect concentrations. From CrB (Cr_2AlB_2) to Cr_3B_4 (Cr_3AlB_4), and to Cr_2B_3 (Cr_4AlB_6), the number of B rings increases. At the same time the vacancy formation energies decrease, which can be attributed to weakening of the Cr-B bonds. With increasing the number of B rings, the defect formation energies of Cr interstitials also decrease in the binary systems, because Cr atoms within B-ring layers form bonds that are softer than Cr atoms outside of the B-ring layers. As a result, Cr within the B-ring layers can accommodate interstitials with a lower energy cost. The defect formation energies of B interstitials in the binary systems showed insignificant changes, and the defect formation energies of all the interstitials in the ternary systems showed a slight decrease with the number of B rings. Based on our results it can be concluded that increasing the number of B rings leads to lower defect formation energies and thus higher concentrations of FPs in the binary and ternary systems. This work lays a foundation and is a necessary step toward understanding defect-related properties of binary borides and ternary MAB phases, which all form different kinds of B networks.

ACKNOWLEDGMENT

The authors gratefully acknowledge support from the Department of Energy Basic Energy Science Program (Grant No. DEFG02–08ER46493).

[1] S. Okada, K. Kudou, K. Iizumi, K. Kudaka, I. Higashi, and T. Lundström, Single-crystal growth and properties of CrB, Cr_3B_4, Cr_2B_3 and CrB_2 from high-temperature aluminum solutions, J. Cryst. Growth **166**, 429 (1996).

[2] X. Zhang, X. Luo, J. Han, J. Li, and W. Han, Electronic structure, elasticity and hardness of diborides of zirconium and hafnium: First principles calculations, Comput. Mater. Sci. **44**, 411 (2008).

[3] W. G. Fahrenholtz and G. E. Hilmas, Ultra-high temperature ceramics: Materials for extreme environments, Scr. Mater. **129**, 94 (2017).

[4] M. Ade and H. Hillebrecht, Ternary borides Cr_2AlB_2, Cr_3AlB_4, and Cr_4AlB_6: The first members of the series $(CrB_2)NCrAl$ with $n = 1, 2, 3$ and a unifying concept for ternary borides as MAB-phases, Inorg. Chem. **54**, 6122 (2015).

[5] H. Xiang, Z. Feng, Z. Li, and Y. Zhou, Theoretical investigations on mechanical and dynamical properties of MAlB (M = Mo, W) nanolaminated borides at ground-states and elevated temperatures, J. Alloys Compd. **738**, 461 (2018).

[6] J. Wei, L. Zhang, and Y. Liu, First-principles calculations study the mechanical and thermal properties of Cr–Al–B ternary borides, Solid State Commun. **326**, 114182 (2021).

[7] Y. Zhou, H. Xiang, F. Z. Dai, and Z. Feng, Electrical conductive and damage-tolerant nanolaminated MAB phases Cr_2AlB_2, Cr_3AlB_4 and Cr_4AlB_6, Mater. Res. Lett. **5**, 440 (2017).

[8] X. Tan, P. Chai, C. M. Thompson, and M. Shatruk, Magnetocaloric effect in $AlFe_2B_2$: Toward magnetic refrigerants from earth-abundant elements, J. Am. Chem. Soc. **135**, 9553 (2013).

[9] O. Shi, L. Xu, A. Jiang, Q. Xu, Y. Xiao, D. Zhu, S. Grasso, and C. Hu, Synthesis and oxidation resistance of MoAlB single crystals, Ceram. Int. **45**, 2446 (2019).

[10] H. Zhang, H. Xiang, F. Z. Dai, Z. Zhang, and Y. Zhou, Oxidation behavior and thermal stability of Cr_2AlB_2 Powders, Corros. Sci. **176**, 108941 (2020).

[11] H. Zhang, J. Y. Kim, R. Su, P. Richardson, J. Xi, E. Kisi, J. O'Connor, L. Shi, and I. Szlufarska, Defect behavior and radiation tolerance of MAB phases (MoAlB and Fe_2AlB_2) with comparison to MAX phases, Acta Mater. **196**, 505 (2020).

[12] Z. Jiang, P. Wang, X. Jiang, and J. Zhao, MBene (MnB): A new type of 2D metallic ferromagnet with high Curie temperature, Nanoscale Horiz. **3**, 335 (2018).

[13] L. T. Alameda, P. Moradifar, Z. P. Metzger, N. Alem, and R. E. Schaak, Topochemical deintercalation of Al from MoAlB: Stepwise etching pathway, layered intergrowth structures, and two-dimensional MBene, J. Am. Chem. Soc. **140**, 8833 (2018).

[14] D. H. Jung, S. J. Yeom, B. M. Kim, Y. J. Lee, and J. T. Kim, Metal line of semiconductor device having a diffusion barrier including Cr_xB_y and method for forming the same, US Patent No. 7,875,979 (2011).

[15] M. Kluge and H. R. Schober, Isotope effect of diffusion in a simple liquid, Phys. Rev. E **62**, 597 (2000).

[16] L. R. Jordan, A. J. Betts, K. L. Dahm, P. A. Dearnley, and G. A. Wright, Corrosion and passivation mechanism of chromium diboride coatings on stainless steel, Corros. Sci. **47**, 1085 (2005).

[17] G. Kresse and J. Furthmüller, Efficient iterative schemes for *ab initio* total-energy calculations using a plane-wave basis set, Phys. Rev. B **54**, 11169 (1996).

[18] G. Kresse and D. Joubert, From ultrasoft pseudopotentials to the projector augmented-wave method, Phys. Rev. B **59**, 1758 (1999).

[19] J. P. Perdew, K. Burke, and M. Ernzerhof, Generalized Gradient Approximation Made Simple, Phys. Rev. Lett. **77**, 3865 (1996).

[20] H. J. Monkhorst and J. D. Pack, Special points for Brillouin-zone integrations, Phys. Rev. B **13**, 5188 (1976).

[21] S. Kota, W. Wang, J. Lu, V. Natu, C. Opagiste, G. Ying, L. Hultman, S. J. May, and M. W. Barsoum, Magnetic properties of Cr_2AlB_2, Cr_3AlB_4, and CrB powders, J. Alloys Compd. **767**, 474 (2018).

[22] M. W. Chase, Jr., *NIST-JANAF Themochemical Tables*, 4th ed. (AIP, Melville, NY, 1998).

[23] See Supplemental Material at http://link.aps.org/supplemental/10.1103/PhysRevMaterials.xx.xxxxxx for (1) justification for neglecting the entropy term in calculations of defect concentrations, (2) range of chemical potentials, (3) additional interstitial structures found in the borides, (4) defect formation energy of all the defects found, (5) concentrations of the most stable defects and Frenkel pairs, and (6) evaluation of available sites per unit volume for each defect for defect concentration calculations.

[24] C. G. Van De Walle and J. Neugebauer, First-principles calculations for defects and impurities: Applications to III-nitrides, J. Appl. Phys. **95**, 3851 (2004).

[25] H. Xu, D. Lee, J. He, S. B. Sinnott, V. Gopalan, V. Dierolf, and S. R. Phillpot, Stability of intrinsic defects and defect clusters in $LiNbO_3$ from density functional theory calculations, Phys. Rev. B **78**, 174103 (2008).

[26] A. F. Kohan, G. Ceder, D. Morgan, and C. G. Van de Walle, First-principles study of native point defects in ZnO, Phys. Rev. B **61**, 15019 (2000).

[27] J. Xi, H. Xu, Y. Zhang, and W. J. Weber, Strain effects on oxygen vacancy energetics in $KTaO_3$, Phys. Chem. Chem. Phys. **19**, 6264 (2017).

[28] F. X. Zhang, J. Xi, Y. Zhang, Y. Tong, H. Xue, R. Huang, C. Trautmann, and W. J. Weber, Local structure and defects in ion irradiated $KTaO_3$, J. Phys.: Condens. Matter **30**, 145401 (2018).

[29] A. Togo and I. Tanaka, First principles phonon calculations in materials science, Scr. Mater. **108**, 1 (2015).

[30] S. Grieshammer and M. Martin, Entropies of defect association in ceria from first principles, Phys. Chem. Chem. Phys. **19**, 29625 (2017).

[31] P. Ágoston and K. Albe, Formation entropies of intrinsic point defects in cubic In_2O_3 from first-principles density functional theory calculations, Phys. Chem. Chem. Phys. **11**, 3226 (2009).

[32] S. Okada, T. Atoda, and I. Higashi, Structural Investigation of Cr_2B_3, Cr_3B_4, and CrB by single-crystal diffractometry, J. Solid State Chem. **68**, 61 (1987).

[33] K. Kádas, D. Iuşan, J. Hellsvik, J. Cedervall, P. Berastegui, M. Sahlberg, U. Jansson, and O. Eriksson, AlM_2B_2 (M = Cr, Mn, Fe, Co, Ni): A group of nanolaminated materials, J. Phys.: Condens. Matter **29**, 155402 (2017).

[34] S. Zhao, J. Xue, Y. Wang, and Q. Huang, *Ab initio* study of irradiation tolerance for different $M_{n+1}AX_n$ phases: Ti_3SiC_2 and Ti_3AlC_2, J. Appl. Phys. **115**, 023503 (2014).